Circuit Modeling Methodology for UWB Omnidirectional Small Antennas

Stanley B. T. Wang, *Member, IEEE*, Ali M. Niknejad, *Member, IEEE*, and Robert W. Brodersen, *Fellow, IEEE*

***Abstract*—In ultra-wideband (UWB) systems, antennas act as filters that introduce a frequency dependent response from the transmitter to receiver. To capture the waveform dispersion so that one can equalize/compensate at the transmitter/receiver, a new circuit modeling methodology that handles omnidirectional small antennas is proposed. By transforming the antennas into the degenerated Foster canonical forms and utilizing the waveform-omnidirectional property, it is shown that the transmitted far field waveform is a scaled version of the voltage across the radiation resistor in the model. Extended Thevenin/Norton equivalent circuits with dependent sources tracking the frequency dependence of the antenna effective length are also built for UWB receiving antennas. Simulation and experimental results show that this methodology is effective over a wide bandwidth and suitable for modeling most UWB antennas.**

***Index Terms*—Antenna transfer function, equivalent circuit, Foster canonical form, small antenna, ultra-wideband (UWB).**

I. INTRODUCTION

IN 2002, the Federal Communications Commission (FCC) released the use of ultra-wideband (UWB) transmission in several frequency bands (0–960 MHz, 3.1–10.6 GHz, and 22–29 GHz) with an effective isotropic radiation power (EIRP) below $-41.3\ \mathrm{dBm/MHz}$ [1]. On one hand, the large bandwidth enables short-range, high data-rate communication [2] and high resolution positioning [3], which are infeasible in narrowband systems; on the other hand, utilization of the large bandwidth imposes new design challenges in UWB systems.

One of the challenges is the design of UWB antennas. It is required that a UWB antenna possess broad impedance bandwidth, high radiation efficiency, small size, omnidirectional radiation pattern (small directivity), and broad radiation pattern bandwidth (or frequency-independent radiation pattern). These properties are generally strong functions of the antenna electrical size. For antennas that are electrically small, the impedance match is poor due to the high quality factor but the radiation pattern is almost constant with frequency; for antennas operating close to the first resonant frequency, the impedance match is good and the radiation pattern is a weak function of frequency; for antennas operating well above the first resonant frequency, the impedance match is good but the radiation pattern changes rapidly with frequency. UWB antenna design is thus about shaping the antenna around the first resonant frequency to achieve simultaneous impedance matching and constant radiation pattern over a wide bandwidth. The state-of-the-art UWB antennas report up to 4:1 impedance bandwidth but less than 3:1 bandwidth meeting both impedance and radiation pattern requirements [4]–[6].

Another challenge is the design of UWB antenna/circuit interface. In traditional narrowband systems, all the design parameters are expressed in single values, i.e., power, gain, reflection coefficient, etc., and the received power can easily be calculated by putting these numbers into Friis transmission formula. Antennas are modeled as resistors with a standard value, say 50 Ω, when designing the interface circuits at the operating frequency. The phase responses of the antennas and radio frequency (RF) front-end circuits are negligible since they are also constants and can be embedded into the channel response and compensated at the receiver. However, in UWB systems, not only are the parameters frequency-dependent, complicating the analysis, but also the whole transmitter-to-receiver transfer function needs to be constructed in order to take into account the waveform dispersion caused by the antennas [7]. The Friis transmission formula is no longer capable of delivering this information for UWB design, and a new methodology needed.

A common way of determining the frequency- and angle-dependent transfer functions is to directly measure or simulate the two-port *S* parameters of the transmitting/receiving antenna pair [8], [9]. Poles and residues can be extracted from *S* parameters to analytically express the transfer function [10]. To make it complete, attempts have been made to simultaneously model the antenna input impedance and transfer function [11], but only the input impedance is modeled by circuit elements while the transfer function is not, which makes it difficult to use for circuit designers. Some software is available for electromagnetic (EM)/circuit cosimulation, but the simulation is time-consuming and it may not support the state-of-the-art transistor models [12]. In this paper, it will be shown that at the transmitter, as long as the antennas operate below a frequency where there is no angular dependency on the radiated waveforms, the input impedance and transfer function are correlated and both of them can be modeled by simple circuit networks. Receiving antenna model can also be built using Thevenin and Norton equivalent circuits.

This paper is organized as follows. Section II first presents the modeling technique for omnidirectional small transmitting antennas, and then examples of a small dipole antenna, a large current radiator, and a circular dipole antenna will be given. Section III covers modeling techniques for omnidirectional small receiving antennas. In Section IV, experimental results for

Manuscript received March 1, 2005; revised September 14, 2005. This work was supported in part by the Army Research Office under Grant 065861, in part by Intel Corporation, and in part by the industrial members of the Berkeley Wireless Research Center. This paper was presented in part at the IEEE APS International Symposium, Monterey, CA, June 2004.

The authors are with Berkeley Wireless Research Center, Department of Electrical Engineering and Computer Science, University of California, Berkeley, CA 94704 USA (e-mail: sbtwang@eecs.berkeley.edu; niknejad@eecs.berkeley.edu; rb@eecs.berkeley. edu).

Digital Object Identifier 10.1109/JSAC.2005.863873

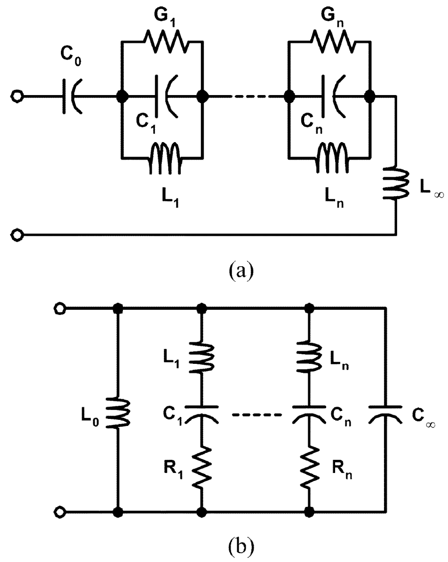

Fig. 1. Foster canonical forms for (a) electric antennas and (b) magnetic antennas.

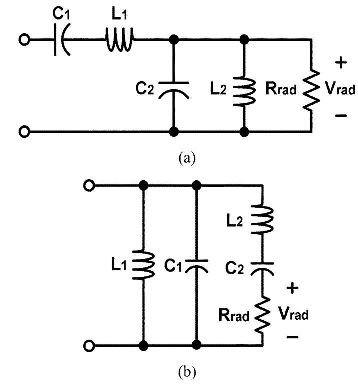

Fig. 2. Degenerated Foster canonical forms for (a) electric antennas and (b) magnetic antennas.

monopole antenna pairs are presented to show the effectiveness of the modeling approach.

II. Modeling Omnidirectional Small Transmitting Antennas

Generally, antennas are linear, passive elements that their input impedances can be represented by Foster canonical forms, as shown in Fig. 1, which follows assuming no ohmic loss [13]. The first Foster canonical form [Fig. 1(a)] is suitable for modeling "electric antennas" like dipole and monopole antennas, and the second Foster canonical form [Fig. 1(b)] is for modeling "magnetic antennas" like loop antennas. The *RLC* tanks in the figures model the resonances of an antenna when the operating frequency increases. For UWB antennas of interest, one operates the antennas in the regime that their radiation pattern is constant with frequency, i.e., below the second resonant frequency, so the Foster canonical forms can be degenerated to that shown in Fig. 2. The circuit topology in Fig. 2(a) has been successfully employed to model the input impedance of dipole antennas [14]. Note that since there is only one resistor in each circuit in Fig. 2, all the power radiated from the antenna is equal to the power dissipated on the resistor, i.e., [15]

$$\frac{V_{\mathrm{rad}}(t-\frac{r}{c})^2}{R_{\mathrm{rad}}} = r^2 \oint_{4\pi} \frac{E(\theta,\phi,r,t)^2}{\eta_0} d\Omega \tag{1}$$

where c is the speed of light, r is the observation distance from the antenna, Ω is the solid angle, η_0 is the free-space characteristic impedance ($= 377\ \Omega$), and $E(\theta,\phi,r,t)$ is the far-zone *E* field propagating in the direction (θ,ϕ). The circuit models can be thought of as a load resistor R_{rad} with an *LC* bandpass filter in the front.

Another property of small antennas is that they are mostly waveform-omnidirectional, i.e., the waveforms of the radiated *E* fields propagating in all directions are the same, and differ only in magnitude. This property is formulated as [15]

$$E(\theta,\phi,r,t) = \alpha(\theta,\phi) \times E(\theta_o,\phi_o,r,t) \tag{2}$$

where $\alpha(\theta,\phi)$ is a direction-dependent scaling factor. Combining (1) and (2) gives

$$\begin{aligned} E(\theta,\phi,r,t) &= -\frac{1}{r}\sqrt{\frac{\eta_0}{\beta R_{\mathrm{rad}}}}\alpha(\theta,\phi)V_{\mathrm{rad}}\left(t-\frac{r}{c}\right) \\ &= \gamma(\theta,\phi,r)V_{\mathrm{rad}}\left(t-\frac{r}{c}\right) \end{aligned} \tag{3}$$

where β and $\gamma(\theta,\phi,r)$ are constants. Once $\gamma(\theta,\phi,r)$ is calculated, one can scale the time-domain voltage V_{rad} across the radiation resistor R_{rad} in the circuit models shown in Fig. 2 and derive waveforms of the radiated *E* fields in any direction. In other words, the transfer function information is embedded in its input impedance.

A. Modeling a Small Dipole Antenna

We first verify the model by considering the simplest antenna—electrically small dipole. It is well known that a small dipole is waveform-omnidirectional, and its far-zone *E* field [15], [16]

$$E_\theta = E_{\theta=90^\circ}\sin\theta. \tag{4}$$

By fitting the input impedance of the circuit in Fig. 2(a) to that of a 6-cm dipole antenna from finite difference time domain (FDTD) simulation [17] using an optimization tool, we obtain $C_1 = 0.68$ pF, $L_1 = 1.24$ nH, $C_2 = 0.64$ pF, $L_2 = 4.91$ nH, and $R_{\mathrm{rad}} = 187\ \Omega$. The resulting impedances from SPICE and FDTD match very well up to 5 GHz, which is almost twice the first resonant frequency. A 0.6-ns-wide Gaussian voltage waveform is then sent into the antenna through a 50-Ω resistor [Fig. 3(a)], and the voltage waveform V_{rad} and the far-zone *E* field at $\theta = 90^\circ$ at 1 m away from the antenna are derived in SPICE and FDTD, respectively. After scaling and time shifting, Fig. 3(b) shows that the two normalized waveforms match well. The ratio of V_{rad} to E_{rad} at 1 m before normalization is 2.2 m. From (1) to (4), β is derived and the theoretical ratio of V_{rad} to E_{rad} at 1 m is 2.0 m, which is within 10% of the simulation results. Further simulation with higher frequency input shows that the model is valid at least up to the antenna's first resonant frequency.

Some insights can be derived from the circuit model. When the frequency is low, the transfer function is approximated as

$$\begin{aligned} \frac{E(\theta,\phi,r)}{V_s} &= \frac{E(\theta,\phi,r)}{V_{\mathrm{in}}} \bullet \frac{V_{\mathrm{in}}}{V_s} \\ &\cong \frac{1}{r}\sqrt{\frac{\eta_0}{R_{\mathrm{rad}}}}\sqrt{\frac{3}{8\pi}}s^2 L_2 C_1 \frac{1}{sC_1R_s+1}. \end{aligned} \tag{5}$$

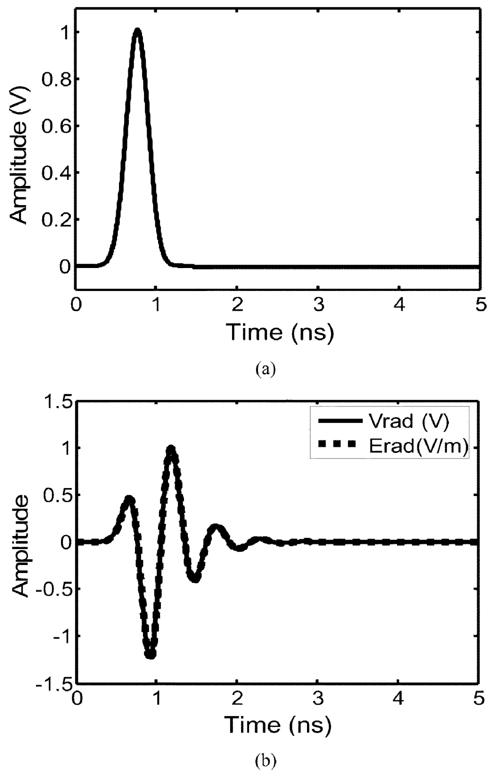

Fig. 3. Time-domain waveforms of the 6-cm dipole antenna. (a) Source voltage waveform with -10-dB bandwidth dc-2 GHz. (b) Normalized $V_{\rm rad}$ from SPICE and $E_{\rm rad}$ (in $\theta = 90^{\circ}$) from XFDTD.

It can be seen that there are two parts involved in the transfer function: one is the impedance division from source voltage V_s to antenna input $V_{\rm in}$; the other is from the antenna input $V_{\rm in}$ to far-zone *E* field. When the source resistance R_s is small, say 50 Ω as in the above case, the transfer function follows a second-derivative relation and is consistent with other UWB antenna analyses on small dipoles [18]. However, when R_s increases, the transfer function will gradually change and the relation eventually becomes closer to first derivative. This means that although the antenna transfer function is fixed, one can still tweak the overall transfer function by setting different impedance value of the driver stage. It is also possible to come up with an equalizer to compensate the filtering effect of the antenna and eliminate the waveform dispersion.

When the operating frequency increases up to the resonant frequency, the reactive parts in the model act as a matching network that transforms radiation resistance $R_{\rm rad}$ to antenna input resistance $R_{\rm in}$. The transfer function thus becomes

$$\frac{E(\theta,\phi,r)}{V_s} \cong \frac{1}{r}\sqrt{\frac{\eta_0}{R_{\rm in}}}\sqrt{\frac{3}{8\pi}}\frac{R_{\rm in}}{R_s+R_{\rm in}} \qquad (6)$$

and a nondispersive radiation is achieved.

B. Modeling a Large Current Radiator

Large current radiators (LCR), such as shown in Fig. 4, have been proposed as UWB antennas [3], [18]. FDTD simulation shows that the resonant frequency of the LCR is about 2 GHz. Since it is a magnetic antenna, the circuit model in Fig. 2(b) is utilized. After curve-fitting the input impedance of the circuit model to that of the LCR, component values are derived as

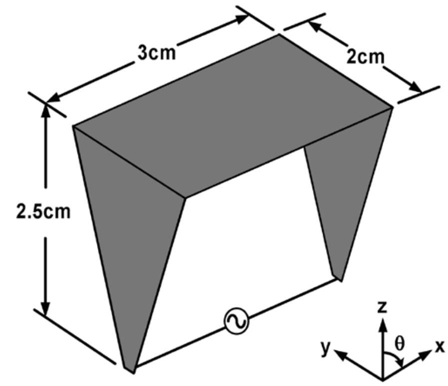

Fig. 4. LCR.

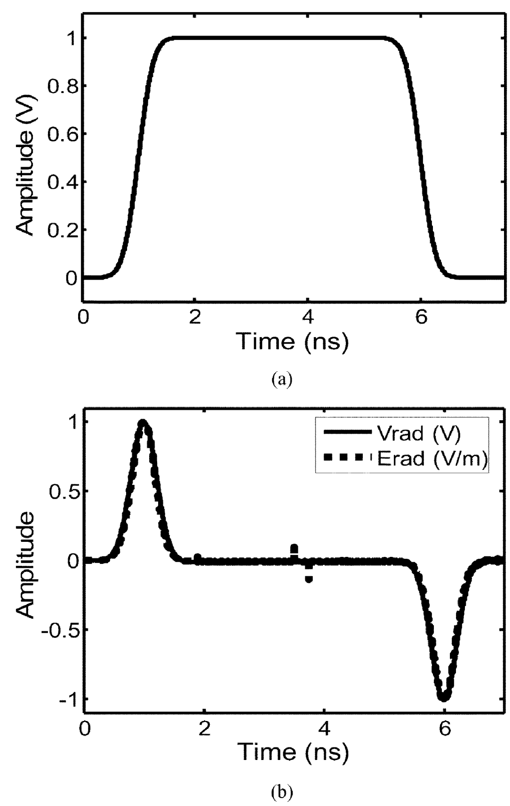

Fig. 5. Time-domain waveforms of the LCR. (a) Source voltage waveform with - 10 dB bandwidth dc-1 GHz. (b) Normalized $V_{\rm rad}$ from SPICE and $E_{\rm rad}$ (in $\theta = 0^{\circ}$) from XFDTD.

$L_1 = 49.4$ nH, $L_2 = 1.65$ nH, $C_2 = 0.13$ pF, $R_{\rm rad} = 31\ \Omega$. Notice that C_1 is ignored since we limit the operating frequency to be below 1 GHz. Driving the antenna by a step function shown in Fig. 5(a) with a source resistance equal to 1 Ω, the normalized waveforms of $V_{\rm rad}$ from SPICE and $E_{\rm rad}$ at $\theta = 0^{\circ}$ from FDTD are derived and shown in Fig. 5(b). Again, the agreement between the waveforms validates the model. The ratio of $V_{\rm rad}$ and $E_{\rm rad}$ is 0.153 m.

Similar to small dipoles, the input voltage to far-zone *E* field transfer function can be formulated for electrically small magnetic antennas

$$\frac{E(\theta,\phi,r)}{V_{\rm in}} \cong \frac{1}{r}\sqrt{\frac{\eta_0}{R_{\rm rad}}}\sqrt{\frac{3}{8\pi}}\frac{sL_1}{sL_1+R_s}sC_2R_{\rm rad}. \qquad (7)$$

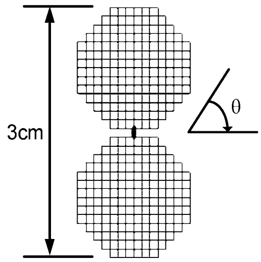

Fig. 6. 3-cm circular dipole antenna.

When the source resistance R_s is small, the transfer function follows a first-derivative relation. When R_s is large, it becomes a second-derivative relation.

C. Modeling a Circular Dipole Antenna

To show that this methodology is not limited to simple electrically small antennas, we also model a circular dipole antenna [19] that has been used in the 3–10-GHz ranges. The antenna geometry is shown in Fig. 6. From FDTD simulation, this antenna self-resonates at 4.3 GHz, and its -10-dB impedance bandwidth is from 3.6 to over 10 GHz. It is waveform-omnidirectional (phase responses overlap and magnitude responses diverge by 3 dB) up to 7 GHz. Because it is an electric antenna, the circuit network from Fig. 2(a) is used. After fitting the input impedance, the circuit component values are derived as $C_1 = 0.58$ pF, $L_1 = 0.85$ nH, $C_2 = 0.53$ pF, $L_2 = 1.5$ nH, and $R_{\text{rad}} = 81\ \Omega$. Figs. 7 and 8 show the simulation results for the antenna driven by a Gaussian and Gaussian-derivative waveforms, respectively. In the first case, input signal -10-dB bandwidth is from direct current (dc) to 5.5 GHz that is 28% greater than its self-resonant frequency [Fig. 7(a)]. The radiated E field at $\theta = 90°$ matches the normalized V_{rad} well [Fig. 7(b)] and the ratio of V_{rad} and E_{rad} is 1.61 m. In the second case, input signal -10-dB bandwidth is from 2 to 11 GHz [Fig. 8(a)]. The high-frequency corner is over twice the self-resonant frequency. It can be seen in Fig. 8(b) that the normalized V_{rad} still makes a reasonable prediction of the far-zone E fields, and behaves like a weighted average of the radiated E fields at $\theta = 90°$ and $\theta = 40°$. It is closer to the E field at $\theta = 90°$ because more power is radiated in that direction.

From the above cases, it is found that the degenerated Foster canonical forms in Fig. 2 are capable of modeling an antenna's input impedance substantially above the first resonant frequency, thus the operating bandwidth of the transmitting antenna model is mainly constrained by the waveform-omnidirectionality that is one of the specifications of good UWB antennas. Therefore, this modeling technique is applicable to most state-of-the-art UWB antennas.

III. Modeling Omnidirectional Small Receiving Antennas

In general, a receiving antenna can be modeled as a Thevenin equivalent circuit with source impedance equal to the antenna impedance and open circuit voltage equal to the incident electric field scaled by a frequency dependent complex factor, i.e., the effective length $\overline{L}_{\text{eff}}$ [13], [16], [20]. In addition, the effective length is also a parameter that relates the radiated E field and the input current when the antenna is transmitting [20], [21]

$$\overline{E} = -j\omega \frac{\mu_0}{4\pi} \frac{e^{-jkr}}{r} \overline{L}_{\text{eff}} I_{\text{in}}. \tag{8}$$

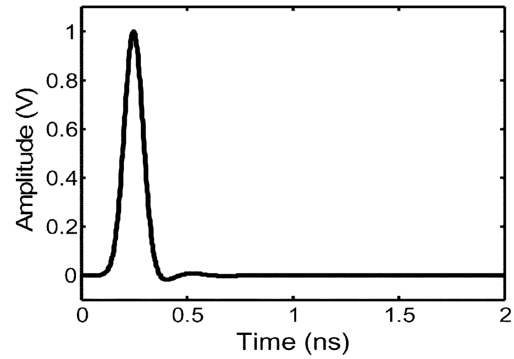

(a)

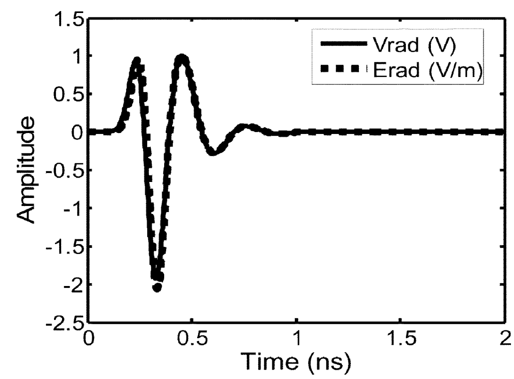

(b)

Fig. 7. Time-domain waveforms of the 3-cm circular dipole antenna. (a) Source voltage waveform with - 10-dB bandwidth dc-5.5 GHz. (b) Normalized V_{rad} from SPICE and E_{rad} (in $\theta = 90°$) from XFDTD.

Considering antennas that can be modeled as Fig. 2(a), if one reformulates (3) in frequency domain and express V_{rad} as a function of I_{in}

$$\overline{E} = -\frac{e^{-jkr}}{r} \sqrt{\frac{\eta_0}{\beta R_{\text{rad}}}} \alpha(\theta, \phi) Z_2 I_{\text{in}} \tag{9}$$

where Z_2 represents the impedance of the parallel tank with C_2, L_2, and R_{rad}. Equating (8) and (9) results in

$$\overline{L}_{\text{eff}} = \frac{\sqrt{\frac{\eta_0}{\beta R_{\text{rad}}}} \alpha(\theta, \phi) Z_2}{j\omega \frac{\mu_0}{4\pi}}. \tag{10}$$

Equation (10) demonstrates that the information of the effective length of an omnidirectional small electric antenna is embedded in the values of C_2, L_2, and R_{rad}. When the frequency is low, Z_2 is dominated by $j\omega L_2$ and $\overline{L}_{\text{eff}}$ becomes a frequency independent constant (L_{eff}), matching the simple equivalent circuit proposed for electrically small antennas in [22]. The antenna impedance is dominated by C_1, and the output voltage of the antenna is

$$\begin{aligned} V_L &= \frac{Z_{\text{ckt}}}{Z_{\text{ant}} + Z_{\text{ckt}}} V_{oc} = \frac{Z_{\text{ckt}}}{Z_{\text{ant}} + Z_{\text{ckt}}} L_{\text{eff}} E_{\text{in}} \\ &= \frac{sC_1 Z_{\text{ckt}}}{1 + sC_1 Z_{\text{ckt}}} L_{\text{eff}} E_{\text{in}}. \end{aligned} \tag{11}$$

Therefore, when the receiver circuit load is a small resistance, the transfer function from the incident E field to the output

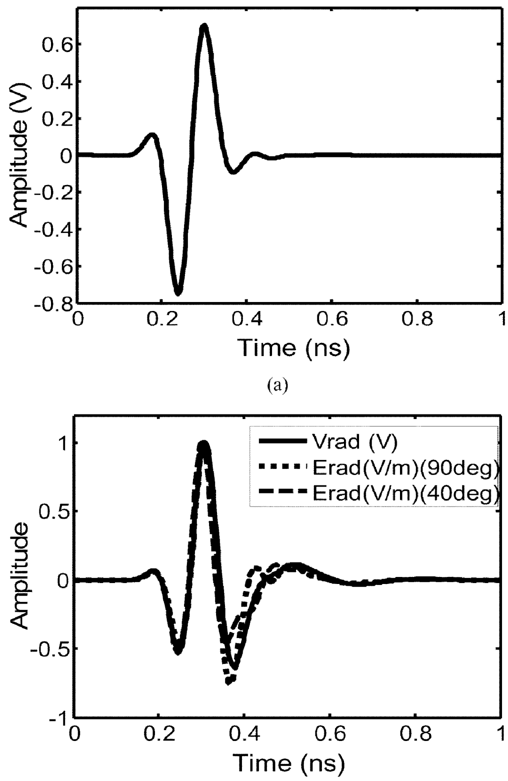

Fig. 8. Time-domain waveforms of the 3-cm circular dipole antenna. (a) Source voltage waveform with - 10-dB bandwidth 2–11 GHz. (b) Normalized $V_{\rm rad}$ from SPICE and $E_{\rm rad}$ (in $\theta = 90°$) from XFDTD.

voltage follows a first-derivative relation. When the load impedance is large compared to C_1, it approaches a linear relation without dispersion. Waveform dispersion may also be eliminated by adopting a capacitive load. When the frequency increases, the change of Z_2 contributed by C_2 and $R_{\rm rad}$ reflects the nonuniformity of the induced currents on the antenna and results in $\overline{L}_{\rm eff}$'s deviation from a real value. Theoretically, the valid operating frequency range of this improved receiving antenna model is the same as that of the corresponding transmitting model, which is beyond the first resonant frequency.

Similar procedure can be taken to derive $\overline{L}_{\rm eff}$ for small magnetic antennas. In contrast to electric antennas, when the frequency is low and the receiver circuit load is a large resistance, the transfer function from the incident *H* field to the output current follows a first-derivative relation. When the load impedance is small, it approaches a linear relation without dispersion. Waveform dispersion may also be eliminated by adopting an inductive load.

Although picking the right circuit loading can preserve the UWB waveform, it is far from ideal in terms of power transfer because the impedances are not matched. The ohmic loss of the antenna, thus far ignored, may also lead to a large noise figure of the antenna and severely degrades the receiver performance. If the frequency is increased to its first resonance and assuming that $L_{\rm eff}$ does not deviate from a real constant too much, the transfer function is

$$V_L = \frac{Z_{\rm ckt}}{Z_{\rm ant} + Z_{\rm ckt}} V_{oc} = \frac{R_{\rm ckt}}{R_{\rm ant} + R_{\rm ckt}} L_{\rm eff} E_{\rm in}. \tag{12}$$

Hence, similar to the case in transmitter, operating the receiving antenna near the first resonant frequency enables the possibility

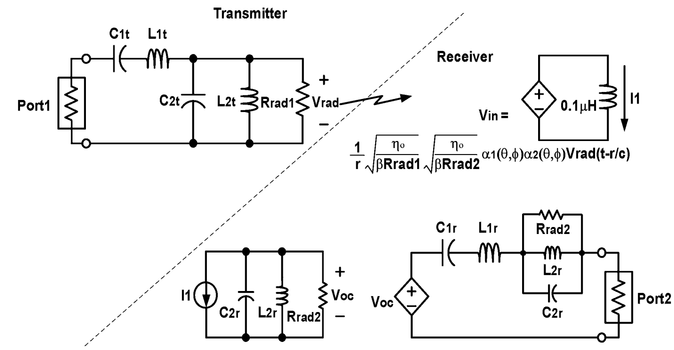

Fig. 9. Complete transmitter-to-receiver antenna model for omnidirectional small electric antennas.

of simultaneous power-match and nondispersive signal reception, which is the optimal approach to take.

The complete transmitter-to-receiver antenna circuit model for omnidirectional small electric antennas is shown in Fig. 9. Two voltage controlled voltage sources and a current controlled current source are utilized to fulfill the transfer function including the impedance ratio in $\overline{L}_{\rm eff}$ expression. The transimpedance Z_{21} can be written as

$$Z_{21} = \frac{1}{r} Z_{2t} \sqrt{\frac{\eta_0}{\beta R_{\rm rad1}}} \sqrt{\frac{\eta_0}{\beta R_{\rm rad2}}} \alpha_1(\theta,\phi)\alpha_2(\theta,\phi) \frac{Z_{2r}}{j\omega \frac{\mu_0}{4\pi}}. \tag{13}$$

If the transmitting and receiving antennas are swapped, the reversed transimpedance Z_{12} can be derived and will be found equal to Z_{21}, which means reciprocity holds in the model. Simple modification can be applied to get alternative circuit models for omnidirectional small magnetic antennas.

IV. Measurement Results of Monopole Antennas

In order to demonstrate the effectiveness of the modeling methodology, monopole antennas with various lengths (1.5, 2.5, and 3.5 cm) are paired up for line-of-sight transmission and the two-port *S* parameters were measured with an HP8719 network analyzer. A rectangular metal plate with dimension 1.1 m by 0.5 m is employed as the ground plane, which isolates the measurement equipments underneath and reduces interference and multipath effects. The distance between the two antennas is 1.05 m. One-port *S* parameters of the monopoles are first taken to obtain the antenna impedances. Model parameters are then derived by curve fitting. As shown in Fig. 10, a nice fit between the models and measurement results are achieved from 50 MHz to 5 GHz for the 1.5- and 2.5-cm monopoles and from 50 MHz to 4 GHz for the 3.5-cm monopole, which implies that the circuit model is able to match the antenna impedances beyond the second resonant frequency. With the assumption that the radiation pattern of the monopole antennas follows a sinusoidal function as in (4), $\alpha(\theta,\phi)$ can be calculated. Two-port *S* parameters can then be predicted using the antenna models shown in Fig. 9 and compared to that from measurements.

Fig. 11 shows the S_{21} (same as S_{12}) data between two 1.5-cm monopole antennas from measurement and our prediction. Both the magnitude and phase responses match well up to 6 GHz—significantly beyond the first resonant frequency. The magnitude response peaks at the first resonant frequency due to better match to 50 Ω. The same procedure is taken

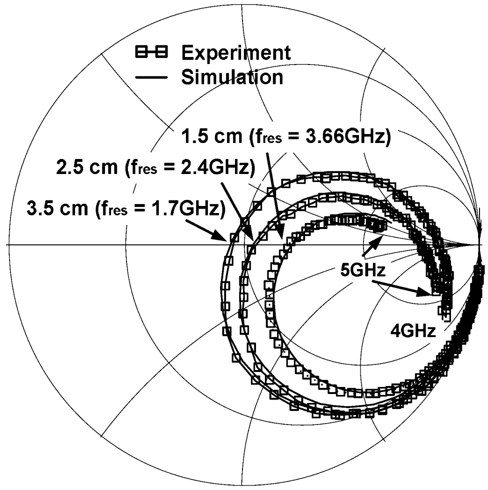

Fig. 10. Measured and simulated S_{11} of 1.5-, 2.5-, and 3.5-cm monopoles.

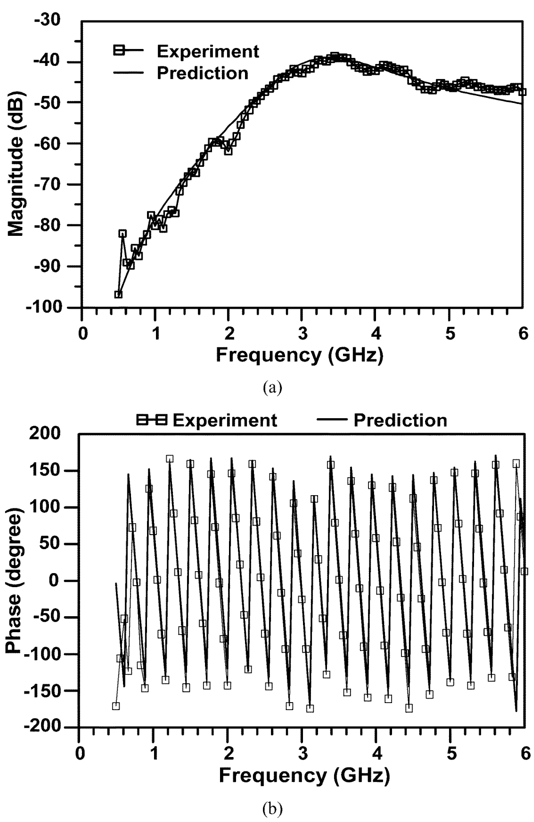

Fig. 11. Measured and predicted *S* parameters of a 1.5-cm monopole antenna pair. (a) Magnitude response of S_{21}. (b) Phase response of S_{21}.

in between the 2.5- and 3.5-cm monopoles and the results are shown in Fig. 12. Two models are built to predict the transfer function: a 2.5-cm monopole transmitter and a 3.5-cm monopole transmitter. As predicted in the previous section, due to reciprocity, the two simulated frequency responses overlap exactly, and both of them match well with the experimental results up to 6 GHz, which is beyond the antennas' second resonant frequencies.

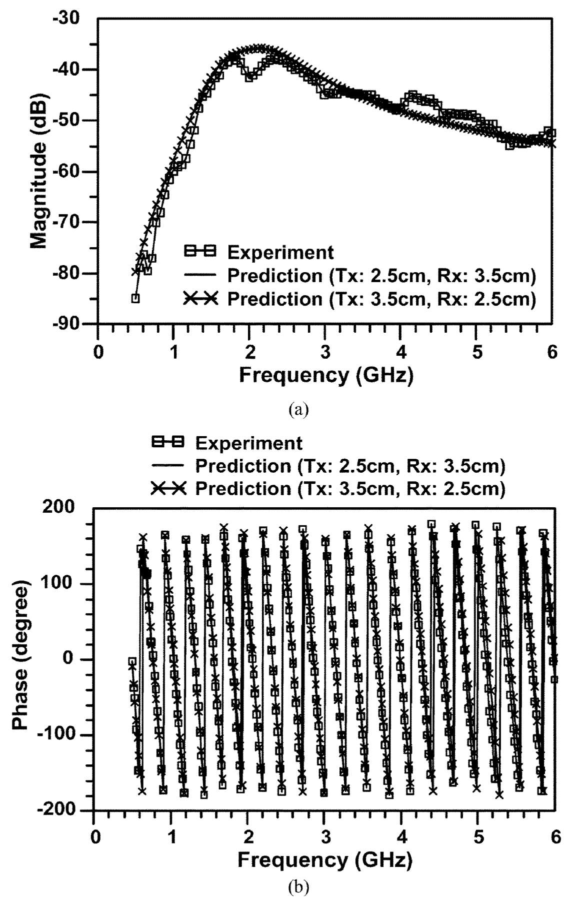

Fig. 12. Measured and predicted *S* parameters of a 2.5-cm/3.5-cm monopole antenna pair. (a) Magnitude response of S_{21}. (b) Phase response of S_{21}.

V. Conclusion

A circuit modeling methodology for UWB omnidirectional small antennas on both the transmitting and receiving sides has been proposed and verified by simulations and measurements. It is able to model the antenna/circuit interface and the corresponding transfer functions by circuit simulators. It is shown that in addition to the antenna dispersion, varying the interface circuit impedance may also lead to different levels of wave shaping, which can be predicted by this model. It is, therefore, possible to do waveform design by choosing nonstandard driver impedance. The approach verifies that operating the antenna close to the first resonant frequency is still the optimal approach in terms of power match and nondispersive transmission.

Acknowledgment

The authors thank I. O'Donnell and M. Chen at BWRC, R. Fleming and C. Kushner at A. Wire & Location, Inc., and Prof. D. Schaubert and Prof. D. Pozar at the University of Massachusetts for their valuable suggestions. The authors are also grateful to Prof. T. G. Ma at National Taiwan University of Science and Technology (NTUST) for the valuable discussion and help on improving the manuscript. Assistance from Y. H. Chee during the measurement is appreciated.

REFERENCES

[1] "Revision of Part 15 of the Commission's rules regarding ultra-wideband transmission systems," FCC Notice of Proposed Rule Making, ET-Docket 98-153.

[2] IEEE 802.15.3a Task Group. [Online]. Available: http://www.ieee802.org/15/pub/TG3a.html

[3] R. Fleming and C. Kushner. Integrated ultra-wideband localizers. presented at 1999 UWB Conference. [Online]. Available: http://www.aetherwire.com

[4] S. Suh, W. Stutzman, W. Davis, A. Waltho, and J. Schiffer, "A novel CPW-fed disc antenna," in *IEEE AP-S Int. Symp. Dig.*, vol. 3, Monterey, CA, Jun. 2004, pp. 2919–2922.

[5] T. G. Ma and S. K. Jeng, "Planar miniature tapered-slot-fed annular slot antennas for ultra-wideband radios," *IEEE Trans. Antennas Propag.*, vol. 53, no. 3, pp. 1194–1202, Mar. 2005.

[6] H. G. Schantz, "Bottom fed planar elliptical UWB antennas," in *Proc. IEEE Conf. Ultra-Wideband Syst. Technol.*, Nov. 2003, pp. 219–223.

[7] Z. N. Chen, X. H. Wu, N. Yang, and M. Y. W. Chia, "Considerations for source pulses and antennas in UWB radio systems," *IEEE Trans. Antennas Propag.*, vol. 52, no. 7, pp. 1739–1748, Jul. 2004.

[8] S. Licul and W. A. Davis, "Ultra-wideband (UWB) antenna measurements using vector network analyzer," in *IEEE APS Int. Symp. Dig.*, vol. 2, Monterey, CA, Jun. 2004, pp. 1319–1322.

[9] X. Qing and Z. N. Chen, "Transfer functions measurement for UWB antennas," in *IEEE APS Int. Symp. Dig.*, vol. 3, Monterey, CA, Jun. 2004, pp. 2532–2535.

[10] S. Licul and W. A. Davis, "Pole/residue modeling of UWB antenna systems," in *IEEE APS Int. Symp. Dig.*, vol. 2, Monterey, CA, Jun. 2004, pp. 1748–1751.

[11] I. Pele, A. Chousseaud, and S. Toutain, "Simultaneous modeling of impedance and radiation pattern antenna for UWB pulse modulation," in *IEEE APS Int. Symp. Dig.*, vol. 2, Monterey, CA, Jun. 2004, pp. 1871–1874.

[12] LC Version 2.10. [Online]. Available: http://lc.cray.com

[13] S. Ramo, J. R. Whinnery, and T. Van Duzer, *Fields and Waves in Communication Electronics*. New York: Wiley, 1994.

[14] M. Hamid and R. Hamid, "Equivalent circuit of dipole antenna of arbitrary length," *IEEE Trans. Antennas Propag.*, vol. 45, no. 11, pp. 1695–1696, Nov. 1997.

[15] S. Wang, A. Niknejad, and R. Brodersen, "Modeling omnidirectional small antennas for UWB applications," in *IEEE APS Int. Symp. Dig.*, vol. 2, Monterey, CA, Jun. 2004, pp. 1295–1298.

[16] D. Cheng, *Field and Wave Electromagnetics*. New York: Addison Wesley, 1989.

[17] Remcom XFDTD v5.1.

[18] J. Taylor, *Introduction to Ultra-Wideband Radar Systems*. Boca Raton, FL: CRC, 1995.

[19] H. G. Schantz, "Planar elliptical element ultra-wideband dipole antennas," in *IEEE APS Int. Symp. Dig.*, vol. 3, Jun. 2002, pp. 16–21.

[20] C. Balanis, *Antenna Theory: Analysis and Design*, 2nd ed. New York: Wiley, 1997.

[21] R. Meys, "A summary of the transmitting and receiving properties of antennas," *IEEE Antennas Propag. Mag.*, vol. 42, no. 3, pp. 49–53, Jun. 2000.

[22] C. Baum, "Parameters for some electrically-small electromagnetic sensors," in *Sensor and Simulations Notes*. Dayton, OH: Air Force Weapons Lab., 1967.

Stanley B. T. Wang (S'96–M'06) received the B.S. and M.S. degrees in electrical engineering from National Taiwan University, Taipei, Taiwan, in 1998 and 2000, respectively, and the Ph.D. degree in electrical engineering from the University of California, Berkeley, in 2005.

His current research is focused on UWB RFIC and antenna design.

Mr. Wang was awarded the Micro Fellowship from 2000 to 2001 and the Intel Robert Noyce Fellowship from 2003 to 2005. He was the recipient of the Best Student Paper Award at the IEEE Radio-Frequency Integrated Circuits Symposium, 2005.

Ali M. Niknejad (S'93–M'00) received the B.S.E.E. degree from the University of California, Los Angeles, in 1994 and the M.S. and Ph.D. degrees in electrical engineering from the University of California, Berkeley, in 1997 and 2000, respectively.

From 2000 to 2002, he worked at Silicon Laboratories, Austin, TX, where he was involved with the design and research of CMOS RF integrated circuits and devices for wireless communication. Presently, he is an Assistant Professor in the Electrical Engineering and Computer Science Department, University of California, Berkeley. He is a Faculty Director at the Berkeley Wireless Research Center (BWRC) and he is the Co-Director of the BSIM Research Group. He serves on the technical program committee of several conferences. His current research interests lie within the area of analog, RF, and microwave integrated circuits, particularly as applied to wireless and broadband communication circuits. His interests also include device modeling and numerical techniques in electromagnetics.

Dr. Niknejad has served as an Associate Editor for the IEEE JOURNAL OF SOLID-STATE CIRCUITS.

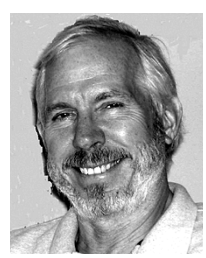

Robert W. Brodersen (M'76–SM'81–F'82) received the Ph.D. degree from the Massachusetts Institute of Technology, Cambridge, in 1972.

He was then with the Central Research Laboratory at Texas Instruments for three years. Following that, he joined the Electrical Engineering and Computer Science Faculty, University of California, Berkeley, where he is now the John Whinnery Chair Professor and Co-Scientific Director of the Berkeley Wireless Research Center. His research is focused in the areas of low-power design and wireless communications and the CAD tools necessary to support these activities.

Prof. Brodersen has won best paper awards for a number of journal and conference papers in the areas of interested circuit design, CAD, and communications, including in 1979 the W. G. Baker Award. In 1983, he was co-recipient of the IEEE Morris Liebmann Award. In 1986, he received the Technical Achievement Awards in the IEEE Circuits and Systems Society and in 1991 from the Signal Processing Society. In 1988, he was elected to be member of the National Academy of Engineering. In 1996, he received the IEEE Solid-State Circuits Society Award and in 1999 received an honorary doctorate from the University of Lund in Sweden. In 2000, he received a Millennium Award from the Circuits and Systems Society, the Golden Jubilee Award from the IEEE. In 2001 he was awarded the Lewis Winner Award for outstanding paper at the IEEE International Solid-State Circuits Conference and in 2003 was given an award for being one of the top ten contributors over the 50 years of that conference.